Investigating Potential Mechanisms for Enhancement of Synchronization in Bushy Cells of the Ventral Cochlear Nucleus

Melih Yayli, Ian C. Bruce

Department of Electrical & Computer Engineering, McMaster University, Hamilton, ON, Canada

McMaster University

Auditory Engineering Laboratory

ABSTRACT

Auditory nerve fibers (ANFs) show synchronous firing to a specific half cycle of the incoming sinusoidal stimuli. This synchronous firing behavior is further enhanced in the bushy cell populations within the ventral cochlear nucleus (VCN; Joris et al., 1994; Joris and Smith, 2008). These cells receive excitatory inputs from ANFs and inhibitory inputs from other cochlear nucleus cell populations such as D-stellate (DS) and tuberculoventral (TV) cells. Anatomical studies have also shown evidence for gap junctions (electrical synapses) between busy cells in both rat (Gómez-Nieto and Rubio, 2009) and rhesus monkey (Gómez-Nieto and Rubio, 2011).

For globular bushy cells (GBC), their enhancement in synchronous firing can be explained by GBC's receiving large numbers of subthreshold ANF inputs and acting as a coincidence detector (Joris and Smith, 2008). For spherical bushy cells (SBC), which have only small numbers of ANF inputs, the mechanism for synchrony enhancement is still unclear. In this study, biophysically detailed neural network models for GBC and SBC microcircuits have been developed based on the model of Manis and Campagnola (2018). The model receives ANF inputs from the phenomenological auditory periphery model of Bruce et al. (2018). We will extend this model to include gap junctions between populations of bushy cells.

I. INTRODUCTION

ANFs demonstrate synchronous firing to low-frequency sinusoidal stimuli. This behaviour can be quantised by the Synchronization Index (SI), which is obtained from the period histogram. If we define h_m as the contents in the m^{th} bin of the period histogram which has M bins, the SI can be estimated as;

$$S_f = (S_{s,f}^2 + S_{c,f}^2)^{1/2} \tag{1}$$

where $S_{s,f}$ and $S_{c,f}$ indicates the sine and cosine components of the SI, which can be calculated by;

$$S_{s,f} = \frac{1}{N}\sum_{m=0}^{M-1} h_m \sin\frac{2\pi m}{M} \quad , \quad S_{c,f} = \frac{1}{N}\sum_{m=0}^{M-1} h_m \cos\frac{2\pi m}{M} \tag{2}$$

N denotes the number of total spike occurrences in the period histogram. SI values range from 0 (flat period histogram) to 1 (only one bin containing all the spikes). The ability of ANFs to show this synchronous firing behaviour depends on several factors such as the spontaneous rate (SR) and characteristic frequency (CF) of the fiber and the frequency and sound pressure level (SPL) of the stimulus.

Several studies have inspected this behaviour for ANFs and bushy cells of the VCN. Studies such as Joris et al. (1994), Joris and Smith (2008) and Spirou et al. (2005) indicate that the synchronous firing behaviour seen in ANFs is enhanced in the SBCs and GBCs. For example, the SI vs SPL plots and raster plots in Fig. 1 show the enhancement in the synchronous firing pattern of BS cells, as measured at their axons in the trapezoid body (TB). Figure 2 shows the maximum SI scores of a population of ANFs with different SR and GBC and SBCs.

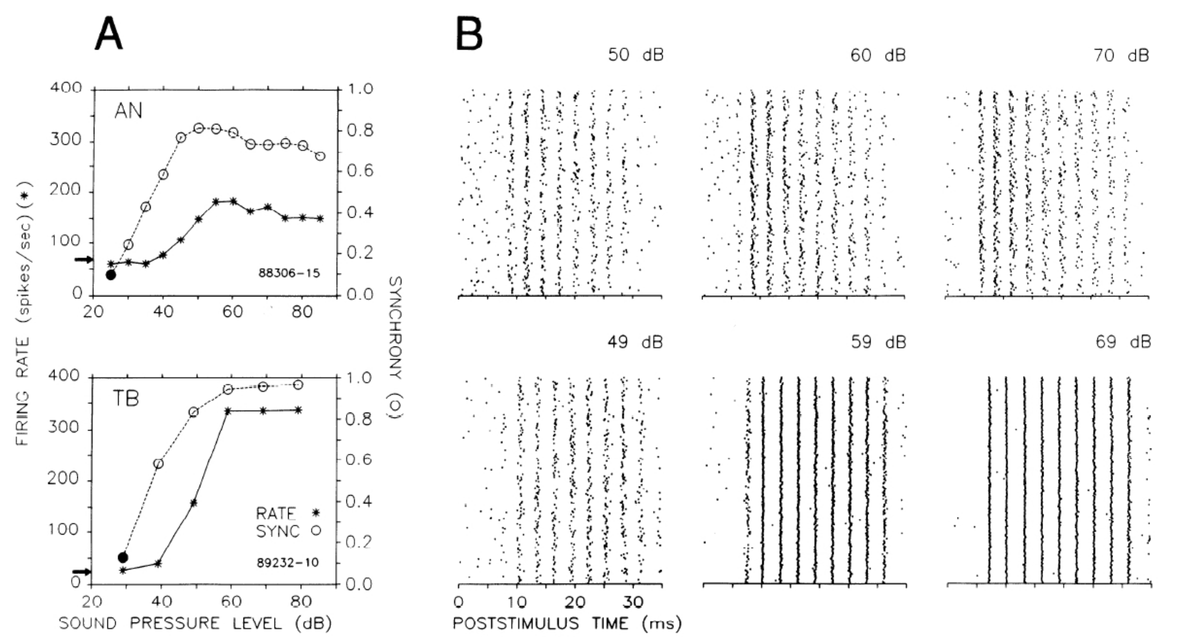

Figure 1: Comparison between ANF (top row) and BC (bottom row) cells' SI scores and firing rates over different SPL. Raster plots are good visualization tools in terms of showing the synchronous firing of ANF and bushy cells. Each dots represents a spike in the specific time bin.

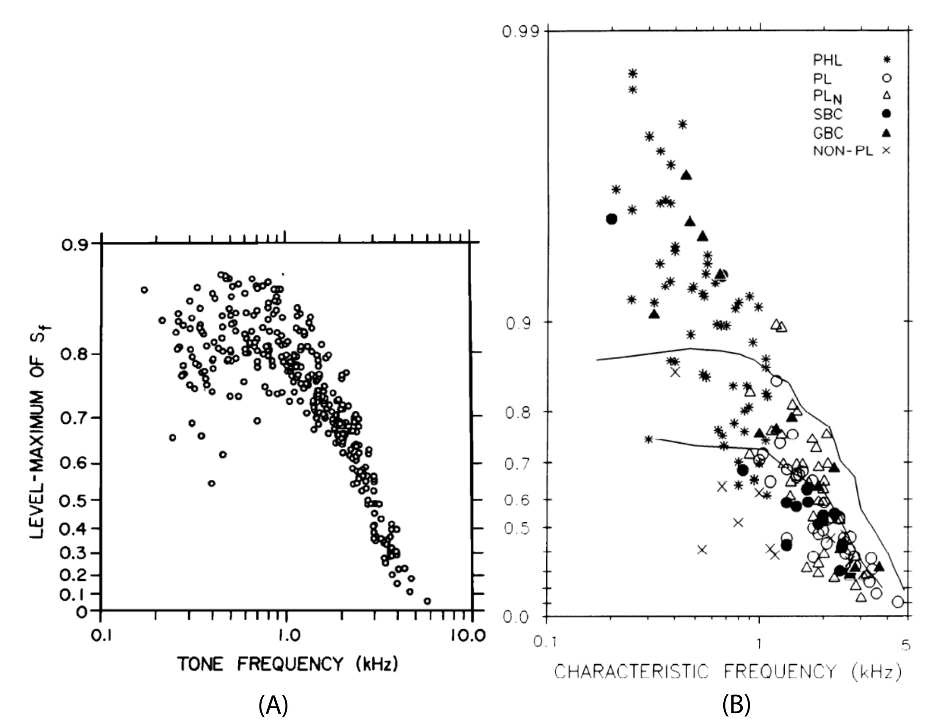

Figure 2: (A) Maximum SI scores of population of ANFs, from Johnson (1980). As the tone frequency increases, the ANF's ability to firing synchronously decreases. The highest score is declared as maximum if the values at neighbouring SPLs are within two standard deviation of the maximum value. (B) Maximum SI scores of cell outputs recorded from the trapezoidal body. The population of cells are a mix of GBCs and SBCs. Some cells are showing close to perfect synchrony (SI $\simeq$ 1) The solid lines indicate the upper and lower boundaries of the reported ANF maximum SI scores. From Joris et al. (1994).

II. METHODS

- Figures 3 and 4 show the VCN microcircuit model used in this study that is based on Manis and Campagnola (2018).

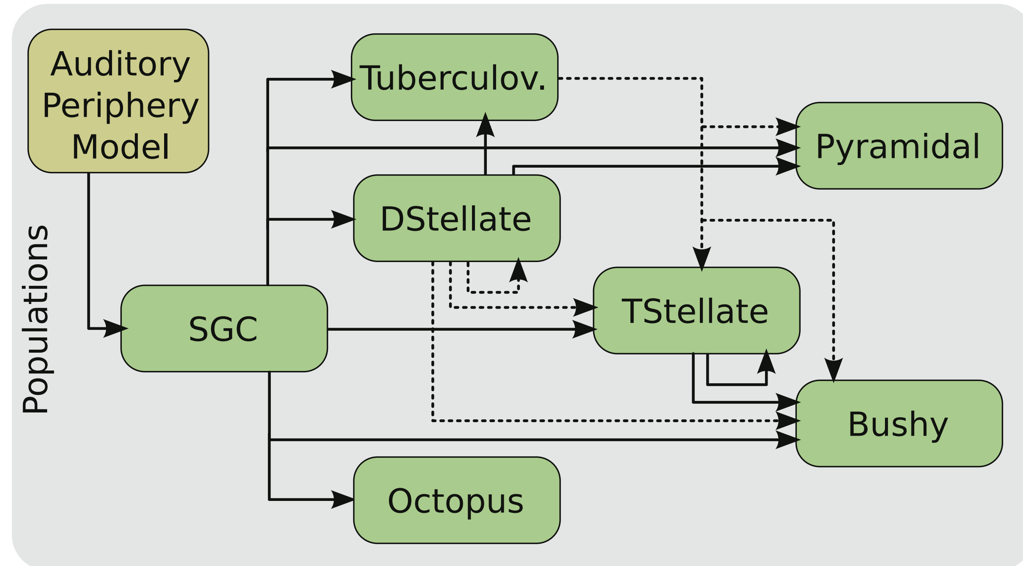

Figure 3: Manis and Campagnola (2018) model of the VCN. Solid lines indicate excitatory connections while dashed lines are inhibitory. The model takes channel equations from NEURON and create cells in a Python environment. Parameters used in this system to create cells and specific connectivity parameters can be found in the repository; `http://www.github.com/cmodel`. From Manis and Campagnola (2018).

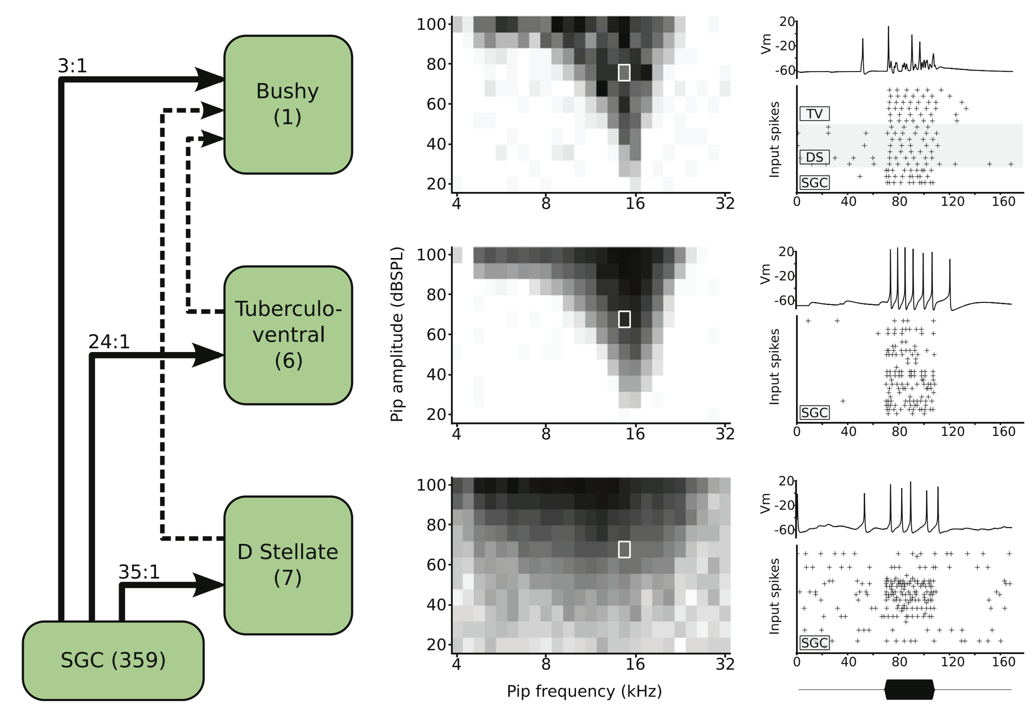

Figure 4: A microcircuit created with Manis and Campagnola (2018) modeling platform. The first layer consists of 7 DS cells receiving input from 35 AN fibers with various SRs. The second layer has 6 TV cells taking excitatory inputs from 24 AN fibers with low and medium SRs. The inhibitory input from DS to TV is disregarded for this simulation. The output bushy cell receives 3 excitatory AN inputs and receives inhibitory inputs from TV and DS cells. The middle column shows the response maps of cells to different frequency and amplitude tone stimuli. Third column shows example firing patterns for a 76 dB SPL, ~15 kHz stimulus. From Manis and Campagnola (2018).

- The microcircuit model is fed by spike trains obtained from the Bruce et al. (2018) AN model.
- To inspect the SI scores of a population of ANFs with different SRs, the procedure defined by Johnson (1980) is followed. Different pure tone stimuli are applied to the population of ANFs containing 80 low, 80 medium and 80 high SR fibers. The stimuli are presented for 15 seconds and the SI is calculated from the period histograms with the method described above.
- The SI calculations of bushy cell types are performed according to Joris et al. (1994). A 350-Hz pure tone stimulus is applied repeatedly for 25 ms followed by a 75-ms silent period for a total recording duration of 20 seconds. The structure of the microcircuit is matched with the microcircuit presented in Fig. 4. The synaptic convergence number and range parameters are introduced in Tables 1 and 2, respectively.

Table 1: Synaptic Convergence Parameters (number of cells)

	Model Type					
	bushy	tstellate	dstellate	octopus	pyramidal	tuberculoventral
ANF	3.3	6.5	35	60	48	24
dstellate	7	20	3	0	15	15
tstellate	0	0	0	0	0	0
tuberculoventral	6	6	0	0	21	0
pyramidal	0	0	0	0	0	0

Table 2: Synaptic Convergence Range Parameters (octaves)

	Model Type					
	bushy	tstellate	dstellate	octopus	pyramidal	tuberculoventral
ANF	0.05	0.1	0.4	0.5	0.1	0.1
dstellate	0.208	0.347	0.5	0	0.2	0.2
tstellate	0.1	0.1	0	0	0	0
tuberculoventral	0.069	0.111	0	0	0.15	0
pyramidal	0	0	0	0	0	0

III. RESULTS

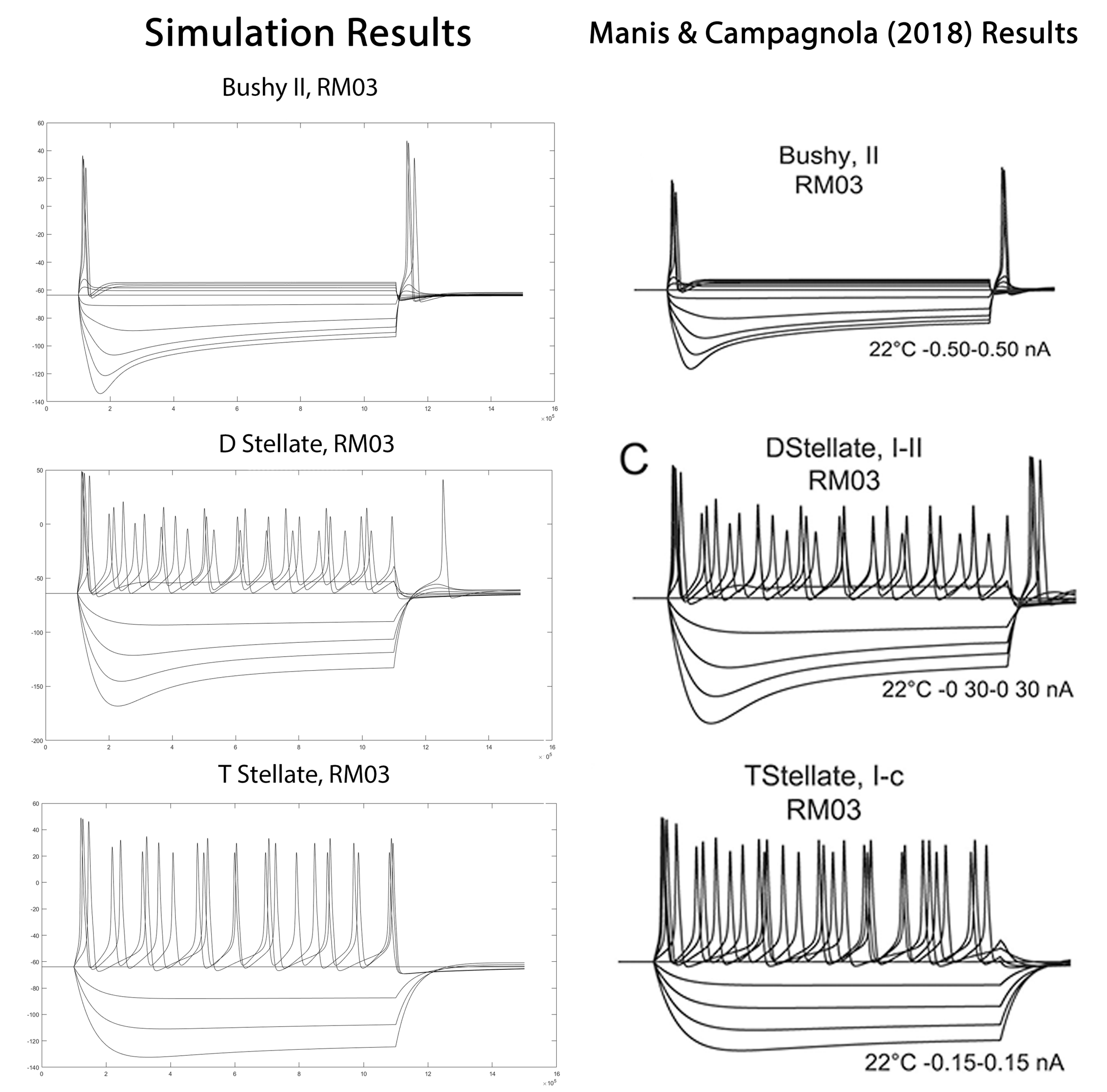

Figure 5: Comparison of current injection simulation results with cell model results presented in Manis and Campagnola (2018). The simulation results are in line with the physiological recordings which confirms that the cell models and mechanisms used in the modeling platform are working properly.

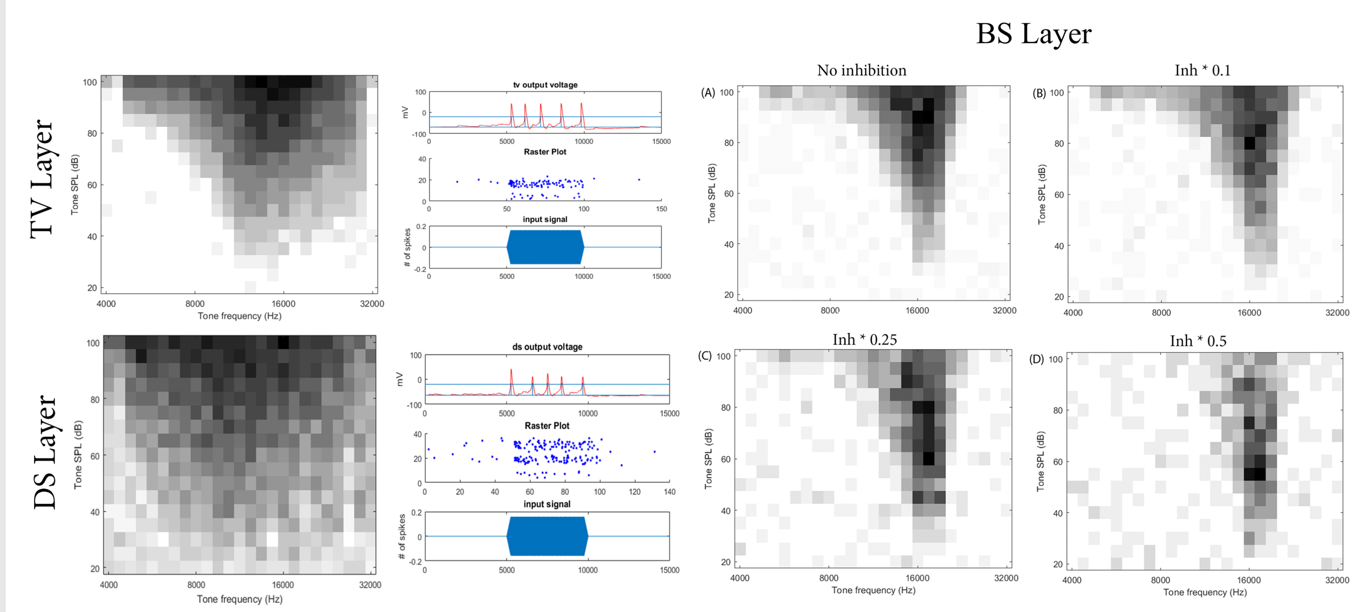

Figure 6: Response maps for our model DS and TV cells, based on the circuit of Manis and Campagnola (2018). The middle column shows an iteration of the simulation when the stimulus intensity is 75 dB and the frequency is 14.672 kHz. Top panels show the membrane voltage of cells and spike trains created from them. Middle panels show the raster plot of AN inputs. Bottom panels show the input tone burst. The right side of the figure shows our model bushy cell response map for different inhibitory input configurations. (A) No inhibition, 3 suprathreshold AN inputs are applied. (B) With inhibition from DS and TV cells multiplied by 0.1. (C) The inhibitory multiplier raised to 0.25. (D) The inhibitory multiplier raised to 0.5.

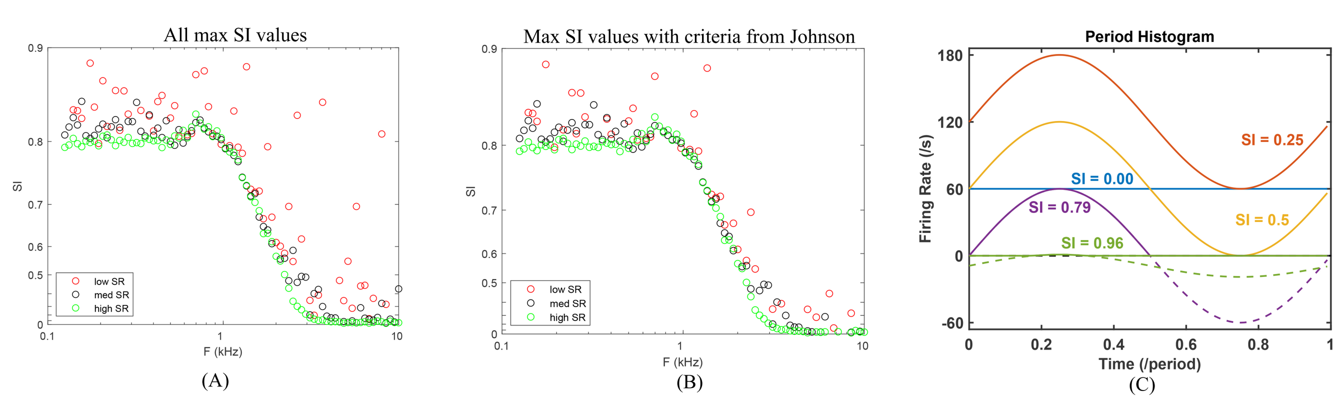

Figure 7: (A) The simulation results of maximum SI scores produced by a population of model AN fibers with different SRs. Low SR fibers tend to have higher SI than the high SR fibers. The highest score of SI is accepted as maximum without any constraints. As a result, some scores on low SR fibers are unexpectedly high at high frequencies. (B) The simulation results of maximum SI scores produced by a population of model AN fibers with different SRs, now applying the criteria defined by Johnson (1980). The upper and lower boundaries are matching with the results presented in Johnson (1980) and Joris et al. (1994). (C) The effect of SR on SI scores. Here we see that high SRs tend to lead to lower SI scores.

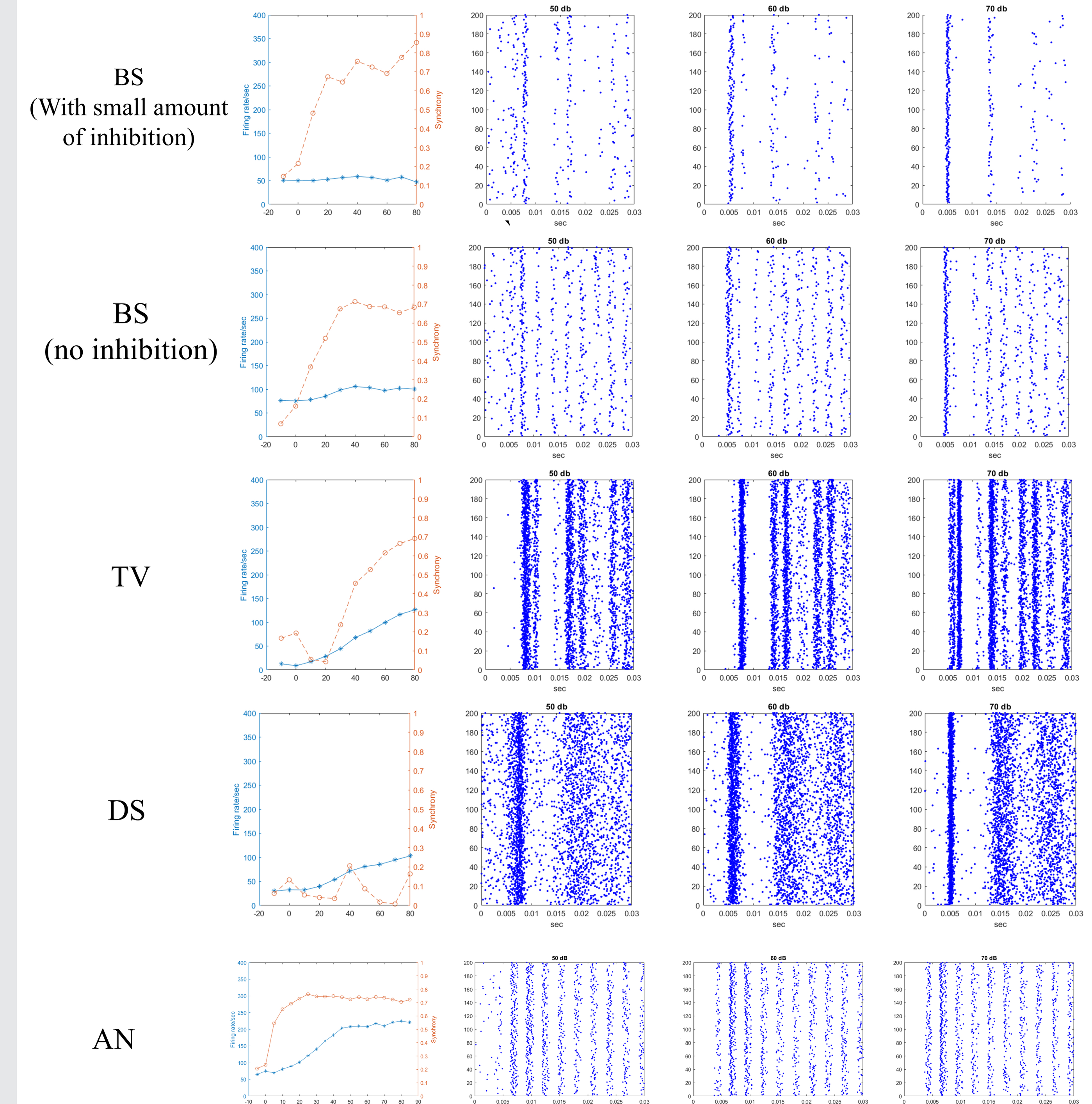

Figure 8: SI, firing rate and raster plots from simulation of the VCN microcircuit based on Manis and Campagnola (2018). Top two levels show the SBC outputs with and without the inhibition. The inhibition provided to the system is obtained from DS and TV layers. Preliminary results show that the inhibition suppresses the spontaneous firing of the bushy cell. As a result, the overall firing rate decreases but the SI score is increased.

IV. CONCLUSIONS

- Our modeling results demonstrate that SR class affects the synchronous firing behaviour of ANF fibers to pure tone stimuli. High SR fibers tend to have lower SI scores since the high number of spontaneous firing results in a broader period histogram. In contrast, low SR fibers are more successful in synchronizing to the peaks of tonal stimuli.
- Preliminary results show a small enhancement in the synchronous firing of bushy cell model with respect to ANFs but this is not sustained across all periods of the stimulus. The increase in the SI score when inhibitory inputs are included in the system suggests that inhibition may play a role in the enhancement of synchronous firing.

V. FUTURE WORK

- The VCN cell models used in this study are constructed for 22℃. At this temperature level cell models have slower dynamics. A temperature scaling should be applied to the model parameters to match the recordings taken at the body temperature level of 38℃.
- Potential mechanisms for synchrony enhancement, including the roles of inhibition (broadband and narrowband inhibition provided by DS and TV cells respectively) and gap junctions, will be inspected by using our GBC and SBC microcircuit models.
- The results of this study are expected to provide insight into the mechanisms behind the enhanced synchronization and entrainment properties of bushy cells, which are important for subsequent binaural processing within the superior olivary complex.

REFERENCES

Bruce, I. C., Erfani, Y., and Zilany, M. S. (2018). A phenomenological model of the synapse between the inner hair cell and auditory nerve: Implications of limited neurotransmitter release sites. *Hearing Research*, 360:40–54.

Gómez-Nieto, R. and Rubio, M. E. (2009). A bushy cell network in the rat ventral cochlear nucleus. *Journal of Comparative Neurology*, 516(4):241–263.

Gómez-Nieto, R. and Rubio, M. E. (2011). Ultrastructure, synaptic organization, and molecular components of bushy cell networks in the anteroventral cochlear nucleus of the rhesus monkey. *Neuroscience*, 179:188–207.

Johnson, D. H. (1980). The relationship between spike rate and synchrony in responses of auditory-nerve fibers to single tones. *The Journal of the Acoustical Society of America*, 68(4):1115–1122.

Joris, P. X., Carney, L. H., Smith, P. H., and Yin, T. (1994). Enhancement of neural synchronization in the anteroventral cochlear nucleus. i. responses to tones at the characteristic frequency. *Journal of Neurophysiology*, 71(3):1022–1036.

Joris, P. X. and Smith, P. H. (2008). The volley theory and the spherical cell puzzle. *Neuroscience*, 154(1):65–76.

Manis, P. B. and Campagnola, L. (2018). A biophysical modelling platform of the cochlear nucleus and other auditory circuits: from channels to networks. *Hearing Research*, 360:76–91.

Spirou, G., Rager, J., and Manis, P. (2005). Convergence of auditory-nerve fiber projections onto globular bushy cells. *Neuroscience*, 136(3):843–863.

yaylim@mcmaster.ca |ibruce@ieee.org

Supported by NSERC Discovery Grant #RGPIN-2018-05778.